Calculation of the heat-source function in photophoresis of aggregated spheres

Yu-lin Xu,[1] B. Å. S. Gustafson,[1] F. Giovane,[2] J. Blum,[3] and S. Tehranian[4]
[1]*Department of Astronomy, P.O. Box 112055, University of Florida, Gainesville, Florida 32611-2055*
[2]*Naval Research Laboratory, 4555 Overlook Avenue SW, Washington, D.C. 20375-5320*
[3]*Astrophysikalisches Institut und Universitäts-Sternwarte, Friedrich-Schiller-Universität Jena, Schillergäßchen 3, 07745 Jena, Germany*
[4]*Institute for Computational Sciences and Informatics, MS5C3, George Mason University, Fairfax, Virginia 22030-4444*
(Received 5 February 1999)

We present theoretical results for the source function in photophoresis of an arbitrary aggregate of spheres that are homogeneous and isotropic piecewise. This source function directly represents the distribution of electric fields inside the spheres. Our calculation is based on a rigorous analytic solution to the radiative multisphere-scattering problem developed recently [Y.-l. Xu, Appl. Opt. **34**, 4573 (1995); **36**, 9496 (1997); Phys. Lett. A **249**, 30 (1998)]. When an aggregate degenerates to a single sphere, the results are exactly the same as those given by the Mie theory. We also discuss the numerical techniques necessary for obtaining an accurate numerical solution for the source function. [S1063-651X(99)11808-7]

PACS number(s): 42.25.Bs, 92.60.Mt, 94.10.Gb, 02.30.Gp

I. INTRODUCTION

A great variety of fascinating and sometimes puzzling physical phenomena stem from complicated interactions of small particles with electromagnetic radiation. The conspicuous zodiacal light, the blueness of the clear sky, rainbows across the sky after a thundershower, brilliant colors of colloidal suspensions of metal powders, are all among the optical manifestations of light scattering by small particles. In addition to scattering, particles may also absorb light. Accompanying scattered radiative fields outside scatterers, there are internal fields excited inside the scatterers. When an absorptive particle is illuminated by an intense light beam, the heat transferred from the incident radiation produces an uneven temperature distribution across the particle. It is observed that, when the incident beam has sufficient intensity, a glass sphere may explode at the illuminated side or at the shaded side, depending on the size and material of the sphere. There is an interesting phenomenon called photophoresis recognized first in 1917 by Ehrenhaft [1] in investigating the elementary electric charge. Photophoresis is a terminology connected with the light-dependent motion of gas-suspended particles on paths of varying degrees of complexity. Following Ehrenhaft's initial discovery, many experimental investigations for observing photophoresis were made, for example, by Rubinowitz [2], Hettner [3], Epstein [4], Whytlaw-Gray and Patterson [5], Reiss [6], Ehrenhaft [7], Deguillon [8], Orr and King [9], Arnold and Amani [10], and many others. Gas-suspended spherical particles illuminated by a light beam of sufficient intensity may move away from or toward the light source. Nonspherical particles may travel in closed orbits or migrate on irregular paths reminiscent of magnified Brownian motion. Photophoresis may cause aerosols to rise against the force of gravity or to fall more rapidly than under gravity alone.

Photophoresis, similar to thermophoresis, is a mechanism driving particles' motion resulting from temperature gradients across the particles. Photophoresis is associated with the absorption properties of a particle. The direction and the magnitude of a photophoretic force exerted on a particle depend on the temperature distribution that, in turn, is determined by the source function describing the rate of energy absorption within the particle. Photophoretic force results from momentum transfer between gas molecules and an unevenly heated surface following radiant-energy absorption. This radiometric force is distinct from radiation pressure. The nonuniformity of the temperature distribution on a particle surface plays the key role in introducing the photophoretic force.

Consider a medium defined by the complex dielectric constant ϵ and the magnetic permeability μ, and an electromagnetic field having the only harmonic time dependence of $\exp(-i\omega t)$ with ω being the circular frequency. Then the Maxwell equations in source-free regions are

$$\nabla\times\mathbf{E}=i\omega\mu\mathbf{H},\quad \nabla\times\mathbf{H}=-i\omega\epsilon\mathbf{E}, \tag{1}$$

which leads to

$$\nabla\cdot\mathbf{S}^*=i\omega\left(\frac{\mu}{2}\mathbf{H}\cdot\mathbf{H}^*-\frac{\epsilon^*}{2}\mathbf{E}\cdot\mathbf{E}^*\right), \tag{2}$$

where $\mathbf{S}^*=1/2\,\mathbf{E}\times\mathbf{H}^*$ is the complex Poynting vector, and the asterisk represents the complex conjugate. As clearly stated by Stratton [11], the divergence of the real part of $\mathbf{S}^*$ determines the energy dissipated in heat per unit volume per unit time, which implies that the heat-source function S is given by

$$S=-\mathrm{Re}(\nabla\cdot\mathbf{S}^*). \tag{3}$$

Because ω and μ are real numbers, the real part of $\nabla\cdot\mathbf{S}^*$ involves only the electric field $\mathbf{E}$. For the problem under our consideration, $\mathbf{E}$ is the internal electric field of the scattering particle. This source function is a starting point for any theory for photophoresis and has been first used by Kerker and Cooke [12,13] in their investigation of the photophoresis of single spherical particles. Often used in practical calculations is the normalized source function $B=\mathbf{E}\cdot\mathbf{E}^*/E_0^2$, where E_0 is the magnitude of the incident electric wave. The calculation of B for the case of single spheres has been studied

 © 1999 The American Physical Society

by Dusel *et al.* [14], Greene *et al.* [15], and others, based on the Mie theory that is a rigorous analytic solution to light scattering by a single homogeneous sphere [16–18]. The detailed description of the Mie theory can be found elsewhere [19–21]. For a single homogeneous sphere illuminated by a plane incident wave with given linear polarization, B changes only with the complex refractive index and the size parameter (the circumference-to-wavelength ratio) x of the sphere.

In this paper we discuss the calculation of the heat-source functions of aggregated homogeneous spheres, including the special case of an isolated single sphere. This is based on a recently developed rigorous and complete analytic solution to the multisphere light-scattering problem [22–24]. This multisphere solution has been confirmed by laboratory microwave analog scattering measurements [25,26]. It reduces to exactly the Mie theory for the special aggregates consisting of only one sphere. The source function for a component sphere in an aggregate of more than one spheres is usually quite different from that when the sphere is isolated. In the present paper, Sec. II derives from the related multisphere light-scattering formulation the formulas needed in the calculation of the heat-source function of an aggregate of spheres. Section III discusses the numerical techniques required in the calculation of the source function to assure a satisfactory accuracy for numerical solutions. Section IV presents some practical examples of our numerical results, including the comparison of our results with those by previous authors for the case of single spheres. At last, Sec. V contains discussions.

II. GENERAL FORMULATION

Equations (2) and (3) define the heat-source function as

$$S=-\mathrm{Re}(\nabla\cdot\mathbf{S}^*)=\frac{1}{2}\sigma\mathbf{E}\cdot\mathbf{E}^*, \tag{4}$$

where $\sigma=\mathrm{Re}(i\omega\epsilon^*)$. The complex dielectric constant $\epsilon=\epsilon'+i\epsilon''$ is related to the complex relative refractive index $m=m'+im''$ through the Maxwell's relation $m^2=\epsilon/\epsilon_0$, where ϵ_0 refers to ϵ in free space. This leads to $\mathrm{Re}(i\omega\epsilon^*)=\omega\epsilon''=2\omega m'm''\epsilon_0$, i.e.,

$$\sigma=\frac{4\pi m'm''}{\lambda_0\mu_0 c}, \tag{5}$$

where λ_0 is the wavelength in free space, μ_0 is the magnetic permeability in free space, and $c=1/\sqrt{\mu_0\epsilon_0}$ is the speed of light in free space. The constant σ is in fact the electric conductivity. This is because the imaginary part of the complex relative dielectric constant is defined by $\epsilon''=\sigma/(\omega\epsilon_0)$.

Equation (4) above tells us that the only task in the calculation of the source function of a particle is to solve the internal electric field of the particle. The multisphere light-scattering theory provides a rigorous solution to the internal fields of every component sphere in an aggregate.

A. Scattered electromagnetic fields of aggregated spheres

Electromagnetic scattering by an arbitrary ensemble of spheres has a complete analytical solution [22–24] analogous to the Mie solution for the light scattering by single spheres, although the multisphere formulation is much more complicated. The Mie solution is, in fact, the simplest special case in the multisphere light-scattering theory.

Consider an L-sphere aggregate. In a primary reference system, the centers of the spheres are respectively located at (X^l,Y^l,Z^l), $l=1,2,\ldots,L$. Each (lth) constituent sphere has a size parameter x^l, a complex relative refractive index m^l, and a magnetic permeability μ^l. The spheres are illuminated by a z-propagating monochromatic plane wave with a linear polarization angle β. The harmonic time dependence $\exp(-i\omega t)$ of the incident wave is implied and suppressed. All individual scattered fields from the L spheres $(\mathbf{E}^l_{\mathrm{sca}},\mathbf{H}^l_{\mathrm{sca}})$ can be expanded as infinite series in terms of vector spherical functions in respective sphere-centered and thus displaced reference systems:

$$\mathbf{E}^l_{\mathrm{sca}}=\sum_{n=1}^{N^l}\sum_{m=-n}^{n} iE_{mn}\left[a^l_{mn}\mathbf{N}^{(3)}_{mn}(k_0r^l,\theta^l,\phi^l)+b^l_{mn}\mathbf{M}^{(3)}_{mn}(k_0r^l,\theta^l,\phi^l)\right], \tag{6a}$$

$$\mathbf{H}^l_{\mathrm{sca}}=\frac{k_0}{\omega\mu_0}\sum_{n=1}^{N^l}\sum_{m=-n}^{n} E_{mn}\left[b^l_{mn}\mathbf{N}^{(3)}_{mn}(k_0r^l,\theta^l,\phi^l)+a^l_{mn}\mathbf{M}^{(3)}_{mn}(k_0r^l,\theta^l,\phi^l)\right], \tag{6b}$$

where (r^l,θ^l,ϕ^l) are the spherical polar coordinates of the spherical coordinate system that has its origin at the center of the lth sphere, k_0 is the wave number of the incident wave in free space, and the constant E_{mn} is defined by [22]

$$E_{mn}=E_0 i^n(2n+1)\frac{(n-m)!}{(n+m)!}. \tag{7}$$

In Eqs. (6), the vector spherical functions (i.e., the linearly independent vector field solutions of the vector wave equation) $\mathbf{M}^{(3)}$ and $\mathbf{N}^{(3)}$, are based on the spherical Hankel function of the first kind. In the component form, $\mathbf{M}^{(3)}$ and $\mathbf{N}^{(3)}$ in Eqs. (6) are written as

$$\mathbf{M}^{(3)}_{mn}=\left[\hat{\mathbf{e}}_\theta i\pi_{mn}(\cos\theta^l)-\hat{\mathbf{e}}_\phi\tau_{mn}(\cos\theta^l)\right]h^{(1)}_n(k_0r^l)\exp(im\phi^l), \tag{8a}$$

$$\mathbf{N}^{(3)}_{mn}=\hat{\mathbf{e}}_r n(n+1)P^m_n(\cos\theta^l)h^{(1)}_n(k_0r^l)\frac{\exp(im\phi^l)}{k_0r^l}+\left[\hat{\mathbf{e}}_\theta i\tau_{mn}(\cos\theta^l)+\hat{\mathbf{e}}_\phi i\pi_{mn}(\cos\theta^l)\right]\times\frac{d}{dr^l}\left[r^l h^{(1)}_n(k_0r^l)\right]\frac{\exp(im\phi^l)}{k_0r^l}, \tag{8b}$$

where $(\hat{\mathbf{e}}_r,\hat{\mathbf{e}}_\theta,\hat{\mathbf{e}}_\phi)$ are the basis unit vectors of the spherical coordinate system, P^m_n is the associated Legendre function of the first kind, and the angular functions π_{mn} and τ_{mn} are defined by

$$\pi_{mn}(\cos\theta)=\frac{m}{\sin\theta}P^m_n(\cos\theta),\quad \tau_{mn}(\cos\theta)=\frac{d}{d\theta}P^m_n(\cos\theta). \tag{9}$$

In practical scattering calculations, the multipole expansion of the scattered field from the lth sphere must be truncated at a sufficiently high order of N^l. As suggested by Wiscombe [27], $N^l \approx x^l + 4\sqrt[3]{x^l} + 2$. The partial scattering coefficients, (a^l_{mn}, b^l_{mn}), i.e., the expansion coefficients of the individual scattered fields from each component sphere associated with respective sphere-centered spherical coordinate systems, are solved in a linear system. This linear system is set up by the standard electromagnetic boundary conditions on the spherical surfaces of all component spheres through the generalization of the Mie theory [22]:

$$a^j_{mn} + a^j_n \sum_{l\neq j}^{(1,L)} \sum_{\nu=1}^{N^l} \sum_{\mu=-\nu}^{\nu} (A^{lj}_{mn\mu\nu} a^l_{\mu\nu} + B^{lj}_{mn\mu\nu} b^l_{\mu\nu}) = a^j_n p^j_{mn}, \tag{10a}$$

$$b^j_{mn} + b^j_n \sum_{l\neq j}^{(1,L)} \sum_{\nu=1}^{N^l} \sum_{\mu=-\nu}^{\nu} (B^{lj}_{mn\mu\nu} a^l_{\mu\nu} + A^{lj}_{mn\mu\nu} b^l_{\mu\nu}) = b^j_n q^j_{mn}, \tag{10b}$$

where $j = 1,2,\ldots,L$, $|m| \leqslant n$, and $n = 1,2,\ldots,N^j$. In Eqs. (10), a^j_n and b^j_n are the Mie scattering coefficients of the isolated jth component sphere [19–22]:

$$a^j_n = \frac{\mu_0 m^j \psi_n(y^j)\psi_n'(x^j) - \mu^j \psi_n(x^j)\psi_n'(y^j)}{\mu_0 m^j \psi_n(y^j)\xi_n'(x^j) - \mu^j \xi_n(x^j)\psi_n'(y^j)}, \tag{11a}$$

$$b^j_n = \frac{\mu^j \psi_n(y^j)\psi_n'(x^j) - \mu_0 m^j \psi_n(x^j)\psi_n'(y^j)}{\mu^j \psi_n(y^j)\xi_n'(x^j) - \mu_0 m^j \xi_n(x^j)\psi_n'(y^j)}, \tag{11b}$$

where $y^j = m^j x^j$, ψ_n, and ξ_n are the Riccati-Bessel functions, $\psi_n(\rho) = \rho j_n(\rho)$ with j_n being the spherical Bessel function of the first kind, $\xi_n(\rho) = \rho h^{(1)}_n(\rho)$ with $h^{(1)}_n$ being the spherical Hankel function of the first kind, and the prime indicates the derivative of a function with respect to its argument. The expansion coefficients of the incident field expressed in the jth coordinate system centered on the jth sphere are given by [22,23]

$$p^j_{mn} = \exp(ik_0 Z^j) p^0_{mn}, \quad q^j_{mn} = \exp(ik_0 Z^j) q^0_{mn}, \tag{12}$$

where $p^0_{mn} = q^0_{mn} = 0$ except $|m| = 1$, and

$$p^0_{1n} = q^0_{1n} = \frac{\exp(-i\beta)}{2}, \quad p^0_{-1n} = -q^0_{-1n} = -\frac{\exp(i\beta)}{2n(n+1)}. \tag{13}$$

In Eqs. (10), $A^{lj}_{mn\mu\nu}$ and $B^{lj}_{mn\mu\nu}$ are the vector translation coefficients associated with the translation vector extended from the origin of the lth coordinate system to the origin of the jth coordinate system, i.e., from the center of the lth component sphere to the center of the jth component sphere. The detailed discussion about the analytical representation of these vector addition coefficients and about the necessary numerical techniques for their evaluation can be found elsewhere [28–30].

As shown by Xu [22–24], the multisphere scattering formulation becomes exactly the same as the Mie formulation when it applies to the case of an aggregate of only one sphere. For the Mie case of a single sphere, Eqs. (10) reduce to

$$a_{mn} = a_n p_{mn}, \quad b_{mn} = b_n q_{mn}, \tag{14}$$

because all the terms involving vector translation coefficients $A^{lj}_{mn\mu\nu}$ and $B^{lj}_{mn\mu\nu}$ vanish. Throughout this paper, the superscript indicating the identification number of a component sphere in an aggregate has been suppressed in all equations written specifically for the case of a single sphere, such as Eqs. (14). When $L = 1$, it follows from Eqs. (13) and (14) that

$$a_{mn} = b_{mn} = 0, \ |m| \neq 1, \tag{15a}$$

$$a_{1n} = \frac{a_n}{2}\exp(-i\beta), \quad a_{-1n} = -\frac{a_n}{2n(n+1)}\exp(i\beta), \tag{15b}$$

$$b_{1n} = \frac{b_n}{2}\exp(-i\beta), \quad b_{-1n} = \frac{b_n}{2n(n+1)}\exp(i\beta), \tag{15c}$$

which include explicitly the polarization state, i.e., the linear polarization angle β, of the plane monochromatic incident wave. Despite this β dependence of the scattering coefficients $(a_{\pm 1n}, b_{\pm 1n})$, the amplitude scattering matrix elements and other scattering properties of a Mie sphere are independent of the linear polarization angle β. The reason for this has been clearly shown by Xu and Wang [26] in the noninteracting-scattering (NIS) formulation for an aggregate of spheres. When applied to sphere-aggregates of $L = 1$, the NIS approximation turns out to be precisely the Mie formulation, in which the β dependence is automatically canceled out in the resulting analytical expressions for the scattering properties.

B. Internal electromagnetic fields of aggregated spheres

Analogous to the scattered fields from each individual sphere, the electromagnetic fields inside each sphere can also be expanded in terms of the vector spherical functions:

$$\mathbf{E}^l_{\text{int}} = -\sum_{n=1}^{N^l} \sum_{m=-n}^{n} iE_{mn}[d^l_{mn}\mathbf{N}^{(1)}_{mn}(\rho^l,\theta^l,\phi^l) + c^l_{mn}\mathbf{M}^{(1)}_{mn}(\rho^l,\theta^l,\phi^l)], \tag{16a}$$

$$\mathbf{H}^l_{\text{int}} = -\frac{k^l}{\omega\mu^l}\sum_{n=1}^{N^l} \sum_{m=-n}^{n} E_{mn}[c^l_{mn}\mathbf{N}^{(1)}_{mn}(\rho^l,\theta^l,\phi^l) + d^l_{mn}\mathbf{M}^{(1)}_{mn}(\rho^l,\theta^l,\phi^l)], \tag{16b}$$

where $\rho^l = k^l r^l$, $k^l = m^l k_0$, and the vector spherical functions with the superscript (1) are associated with the spherical Bessel function of the first kind, i.e.,

$$\mathbf{M}^{(1)}_{mn} = [\hat{\mathbf{e}}_\theta i\pi_{mn}(\cos\theta^l) - \hat{\mathbf{e}}_\phi \tau_{mn}(\cos\theta^l)] j_n(\rho^l)\exp(im\phi^l), \tag{17a}$$

$$\mathbf{N}_{mn}^{(1)}=\hat{\mathbf{e}}_r n(n+1)P_n^m(\cos\theta^l)j_n(\rho^l)\frac{\exp(im\phi^l)}{\rho^l}+[\hat{\mathbf{e}}_\theta i\tau_{mn}(\cos\theta^l)+\hat{\mathbf{e}}_\phi i\pi_{mn}(\cos\theta^l)]\frac{d}{dr^l}[r^l j_n(\rho^l)]\frac{\exp(im\phi^l)}{\rho^l}. \tag{17b}$$

There are very simple relations between the internal coefficients (d_{mn}^l,c_{mn}^l) and the scattering coefficients (a_{mn}^l,b_{mn}^l) [22]:

$$d_{mn}^l=\frac{d_n^l}{a_n^l}a_{mn}^l,\quad c_{mn}^l=\frac{c_n^l}{b_n^l}b_{mn}^l, \tag{18}$$

where (d_n^l,c_n^l) are the internal Mie coefficients of the isolated lth sphere [19–22]:

$$d_n^l=\frac{i\mu^l m^l}{\mu_0 m^l\psi_n(y^l)\xi_n'(x^l)-\mu^l\xi_n(x^l)\psi_n'(y^l)}, \tag{19a}$$

$$c_n^l=\frac{i\mu^l m^l}{\mu^l\psi_n(y^l)\xi_n'(x^l)-\mu_0 m^l h_n^{(1)}(x^l)\psi_n'(y^l)}. \tag{19b}$$

With (a_{mn}^l,b_{mn}^l) known, (d_{mn}^l,c_{mn}^l) can be easily calculated from Eqs. (18), (11), and (19), which can be explicitly written as

$$d_{mn}^l=\frac{i\mu^l m^l}{\mu_0 m^l\psi_n(y^l)\psi_n'(x^l)-\mu^l\psi_n(x^l)\psi_n'(y^l)}a_{mn}^l, \tag{20a}$$

$$c_{mn}^l=\frac{i\mu^l m^l}{\mu^l\psi_n(y^l)\psi_n'(x^l)-\mu_0 m^l\psi_n(x^l)\psi_n'(y^l)}b_{mn}^l. \tag{20b}$$

In terms of Eqs. (16), the internal electric field components of the lth sphere in the spherical polar coordinates (r^l,θ^l,ϕ^l) centered at the lth sphere can be written as

$$E_\theta^l=\sum_{n=1}^{N^l}\sum_{m=-n}^{n}E_{mn}(-id_{mn}^l\psi_n'\tau_{mn}+c_{mn}^l\psi_n\pi_{mn})\exp(im\phi^l)/\rho^l, \tag{21a}$$

$$E_\phi^l=\sum_{n=1}^{N^l}\sum_{m=-n}^{n}E_{mn}(ic_{mn}^l\psi_n\tau_{mn}+d_{mn}^l\psi_n'\pi_{mn})\exp(im\phi^l)/\rho^l, \tag{21b}$$

$$E_r^l=\sum_{n=1}^{N^l}\sum_{m=-n}^{n}-iE_{mn}n(n+1)d_{mn}^l P_n^m\psi_n\exp(im\phi^l)/(\rho^l)^2, \tag{21c}$$

where the arguments of ψ_n and ψ_n' are $\rho^l=k^l r^l$.

In the case of $L=1$ for an aggregate of spheres under our consideration, i.e., in the Mie case of a single homogeneous sphere irradiated by a monochromatic z-propagating and linearly polarized plane wave, it follows from Eqs. (18) and (15) that

$$d_{mn}=c_{mn}=0,\ |m|\neq 1, \tag{22a}$$

$$d_{1n}=\frac{d_n}{2}\exp(-i\beta),\quad d_{-1n}=-\frac{d_n}{2n(n+1)}\exp(i\beta), \tag{22b}$$

$$c_{1n}=\frac{c_n}{2}\exp(-i\beta),\quad c_{-1n}=\frac{c_n}{2n(n+1)}\exp(i\beta). \tag{22c}$$

With the use of Eqs. (22) for the special Mie case, Eqs. (21) provide the internal field components of a single Mie sphere:

$$E_\theta=\frac{\cos(\phi-\beta)}{\rho}\sum_{n=1}^{N}E_n(-id_n\psi_n'\tau_n+c_n\psi_n\pi_n), \tag{23a}$$

$$E_\phi=\frac{\sin(\phi-\beta)}{\rho}\sum_{n=1}^{N}E_n(id_n\psi_n'\pi_n-c_n\psi_n\tau_n), \tag{23b}$$

$$E_r=\frac{\cos(\phi-\beta)}{\rho^2}\sum_{n=1}^{N}-iE_n n(n+1)d_n P_n^1\psi_n, \tag{23c}$$

where use has been made of the notations of $\rho=kr$, $E_n=E_{1n}=E_0 i^n(2n+1)/[n(n+1)]$, $\pi_n=\pi_{1n}$, $\tau_n=\tau_{1n}$ and the relations

$$\pi_{-1n}=\frac{\pi_n}{n(n+1)},\quad \tau_{-1n}=-\frac{\tau_n}{n(n+1)}, \tag{24a}$$

$$P_n^{-1}=-\frac{P_n^1}{n(n+1)}, \tag{24b}$$

$$E_{-1n}=i^n E_0(2n+1)n(n+1)=E_n n^2(n+1)^2. \tag{24c}$$

Equations (23) are the same as those given by the Mie theory. But one should pay attention to the appearance of the linear polarization angle β in Eqs. (23), which is often overlooked.

III. CALCULATION OF THE HEAT-SOURCE FUNCTION

As described in the preceding sections, Eqs. (21), the general analytical expressions for internal-field components, and Eqs. (10) for the partial scattering coefficients are the key equations required in the calculation of the heat-source function of aggregated spheres. The numerical solution of the source function mainly involves: (a) solution of the linear equations, Eqs. (10), for the scattering coefficients (a_{mn}^l,b_{mn}^l), (b) calculation of the internal coefficients (d_{mn}^l,c_{mn}^l) through Eqs. (20), and (c) calculation of the internal field components $(E_r^l,E_\theta^l,E_\phi^l)$ through Eqs. (21). This solution requires the evaluation of (a) a large number of vector translation coefficients $(A_{mn\mu\nu}^{lj},B_{mn\mu\nu}^{lj})$, (b) the Mie scattering coefficients of each component sphere (a_n^l,b_n^l), and (c) the Riccati-Bessel functions ψ_n and ψ_n' with both real and complex arguments. The use of appropriate numerical tech-

niques in the evaluation of all these coefficients and special functions is of crucial importance to ensure sufficient accuracy of the numerical solution. As noticed by Greene *et al.* [15] in their calculation of the source function for single Mie spheres, numerical results are sensitive to errors in evaluating the Riccati-Bessel functions used to describe the internal field distribution. Minor errors in the total rate of energy absorption will completely distort the temperature distribution within a particle and the associated photophoretic force. Multisphere calculations are even more complicated. Special attention should be paid to the numerical schemes used in each step of the calculation of the source function. This section discusses numerical aspects in practical calculations of the source function from a technical point of view and describes what we use in our calculations.

A. Evaluation of vector translation coefficients

A reliable calculation of the source function of aggregated spheres depends first on the accurate solution of all partial scattering coefficients (a_{mn}^{l},b_{mn}^{l}). This, in turn, calls for an effective approach to evaluating the vector translation coefficients $(A_{mn\mu\nu}^{lj},B_{mn\mu\nu}^{lj})$ appearing in Eqs. (10) as the coefficient matrix elements of the unknown scattering coefficients (a_{mn}^{l},b_{mn}^{l}). The computation of the vector translation coefficients $A_{mn\mu\nu}^{lj}$ and $B_{mn\mu\nu}^{lj}$ has been discussed in detail by Xu [30]. In the literature there exist three basic types of analytical expressions for these addition coefficients in terms of either the scalar translation coefficients [31], the Wigner $3jm$ symbol [32], or the Gaunt coefficient [33], as formulated by Stein [28], Cruzan [29], and Xu [30,34], respectively. Systematic numerical tests show that these different formulations are equivalent from the point of view of numerical results [30]. Considering the computational efficiency, we use Xu's formulas for $A_{mn\mu\nu}^{lj}$ and $B_{mn\mu\nu}^{lj}$ that are based on the Gaunt coefficient:

$$A_{mn\mu\nu}^{lj}=(-1)^{m}\frac{(2\nu+1)(n+m)!(\nu-\mu)!}{2n(n+1)(n-m)!(\nu+\mu)!}\times\exp[i(\mu-m)\phi_{lj}]\sum_{q=0}^{q_{\max}}i^{p}[n(n+1)+\nu(\nu+1)-p(p+1)]g_{q}h_{p}^{(1)}(kd_{lj})P_{p}^{\mu-m}(\cos\theta_{lj}),\tag{25a}$$

$$B_{mn\mu\nu}^{lj}=(-1)^{m}\frac{(2\nu+1)(n+m)!(\nu-\mu)!}{2n(n+1)(n-m)!(\nu+\mu)!}\exp[i(\mu-m)\phi_{lj}]\sum_{q=0}^{Q_{\max}}i^{p+1}b_{q}h_{p+1}^{(1)}(kd_{lj})P_{p+1}^{\mu-m}(\cos\theta_{lj}),\tag{25b}$$

where $(d_{lj},\theta_{lj},\phi_{lj})$ are the spherical coordinates of the origin of the jth coordinate system in the lth coordinate system, and

$$p=n+\nu-2q,\tag{26a}$$

$$q_{\max}=\min\left(n,\nu,\frac{n+\nu-|\mu-m|}{2}\right),\tag{26b}$$

$$Q_{\max}=\min\left(n,\nu,\frac{n+\nu+1-|\mu-m|}{2}\right).\tag{26c}$$

In Eqs. (25), g_q is the Gaunt coefficient defined by

$$g_{q}=g(-m,n,\mu,\nu,p)=\frac{(2p+1)}{2}\frac{(p+m-\mu)!}{(p-m+\mu)!}\int_{-1}^{1}P_{n}^{-m}(x)P_{\nu}^{\mu}(x)P_{p}^{\mu-m}(x)dx,\tag{27}$$

and

$$b_{q}=\frac{2p+3}{A_{p+2}}[(p+2)(p_{1}+1)\alpha_{p+1}g_{q}-(p+1)(p_{2}+2)\alpha_{p+2}g_{q-1}],\quad A_{p+2}\neq0,\tag{28a}$$

$$b_{q}=\frac{2p+3}{(p+3)(p_{1}+2)A_{p+4}}\{[A_{p+3}A_{p+4}+(p+2)(p+4)(p_{1}+3)(p_{2}+3)\alpha_{p+3}]g_{q-1}-(p+2)(p+3)(p_{2}+3)(p_{2}+4)\alpha_{p+4}g_{q-2}\},\quad A_{p+2}=0,\tag{28b}$$

where

$$A_{p}=(\mu+m)(m-\mu)(n-\nu)(n+\nu+1)-p(p-1)(m+\mu),\tag{29a}$$

$$p_{1}=p+m-\mu,\tag{29b}$$

$$p_{2}=p-m+\mu,\tag{29c}$$

$$\alpha_{p}=\frac{[p^{2}-(n-\nu)^{2}][p^{2}-(n+\nu+1)^{2}]}{4p^{2}-1}.\tag{29d}$$

The evaluation of b_q requires a single set of the Gaunt coefficients $g(-m,n,\mu,\nu,p)$. The general recurrence relations of Gaunt coefficients and the efficient scheme for their accurate and fast recursive evaluation can be found in Xu [30,35,36].

Calculation of vector translation coefficients $(A_{mn\mu\nu}^{lj},B_{mn\mu\nu}^{lj})$ is required only for sphere-aggregates of $L>1$. For a single sphere, translation coefficients are not involved and the calculation of the source function is thus much simpler than in the multisphere case.

B. Evaluation of Riccati-Bessel functions

Calculation of the internal coefficients (d_{mn}^{l},c_{mn}^{l}) from the scattering coefficients (a_{mn}^{l},b_{mn}^{l}) through Eqs. (20) requires the evaluation of the Riccati-Bessel functions $\psi_n(x^l)$, $\psi_n(y^l)$ and their derivatives $\psi_n'(x^l)$, $\psi_n'(y^l)$. Also, the calculation of the internal field components $(E_{r}^{l},E_{\theta}^{l},E_{\phi}^{l})$ for any r^l inside the particle from the calculated internal coefficients d_{mn}^{l} and c_{mn}^{l} using Eqs. (21) requires the values of $\psi_n(k^lr^l)$ and $\psi_n'(k^lr^l)$. To obtain a reliable numerical solution for the source function, one therefore needs a satisfactory scheme to evaluate these Riccati-Bessel functions of both real and complex arguments.

At first glance, the simplest method of computing the Riccati-Bessel functions of all needed orders seems to be the one directly using the recurrence relations

$$\psi_n(z)=\frac{2n-1}{z}\psi_{n-1}(z)-\psi_{n-2}(z), \tag{30a}$$

$$\psi_n'(z)=\psi_{n-1}(z)-\frac{n}{z}\psi_n(z). \tag{30b}$$

Even though the starting values can be calculated accurately through appropriate special methods, forward recursion based on Eqs. (30) is in general numerically unstable and often yields erroneous numerical results, especially for high orders. Kerker [20] suggested the use of backward recursion with starting values at the two highest orders calculated by the series expansion

$$\psi_n(z)=2^n z^{n+1}\sum_{j=0}^{\infty}\frac{(-1)^j(n+j)!z^{2j}}{j!(2n+2j+1)!}. \tag{31}$$

Greene *et al.* used this backward recursion scheme in their study of absorption centers of an irradiated single sphere and published their numerical results for a range of the size parameter from 0.5 to 20 and for some selected refractive indexes [15]. It is found that the numerical accuracy of Greene *et al.*'s results are generally insufficient. This is mainly because the backward recursion is still not satisfactorily reliable. One problem, probably the most obvious, is that the direct use of the series expansion to calculate Riccati-Bessel functions is usually not an appropriate approach, especially at high orders. When the value of the argument is not small, the convergency of the series expansion is not warranted. Ross [37] proposed a method that combines backward and forward recursions by calculating in backward recursion when the function continuously increases until the maximum is reached and then calculating the other part of lower orders in forward recursion when necessary. In this method the starting values at the two highest orders are calculated by the approximate formula

$$\psi_n(z)=\frac{z}{2t\chi_n(z)}, \tag{32}$$

where $\chi_n(z)$ is also a Riccati-Bessel function, $\chi_n(z)=-zy_n(z)$ with $y_n(z)$ being the spherical Bessel function of the second kind, and

$$t=[(n+0.5)^2-z^2]^{1/2}. \tag{33}$$

Dusel *et al.* [14] used this method in their study of the photophoresis of single spheres. We found that Dusel *et al.*'s numerical results are close to ours. This is because Ross' modified backward recursion scheme has to some extent improved the calculation of the Riccati-Bessel functions. Lentz [38] deviced a method of evaluating continued fractions for generating Riccati-Bessel functions and their ratios. In 1991, Wang and van de Hulst [39] presented a very neat algorithm based on the ratio method for computing the Riccati-Bessel functions, which has been used by Wang for both spherical and cylindrical Bessel functions in his Mie-scattering and other scattering calculations since 1973 [39,40]. Wang's method is accurate and reliable. Our calculation of Riccati-Bessel functions is based on this ratio method, which is briefly described below.

In practical calculations of the internal field components of either a Mie sphere or aggregated spheres, the derivative of the Riccati-Bessel function ψ_n' can be replaced by the logarithmic derivative

$$D_n(z)=\frac{d}{dz}\ln\psi_n(z)=\frac{\psi_n'(z)}{\psi_n(z)}, \tag{34}$$

where z is either real or complex. With the use of the logarithm derivative $D_n(z)$, Eqs. (20) have the alternative form

$$d_{mn}^l=\frac{i\mu^l m^l}{\psi_n(x^l)\psi_n(y^l)[\mu_0 m^l D_n(x^l)-\mu^l D_n(y^l)]}a_{mn}^l, \tag{35a}$$

$$c_{mn}^l=\frac{i\mu^l m^l}{\psi_n(x^l)\psi_n(y^l)[\mu^l D_n(x^l)-\mu_0 m^l D_n(y^l)]}b_{mn}^l. \tag{35b}$$

Equations (35) are more convenient than Eqs. (20) in practical calculation of the internal coefficients (d_{mn}^l, c_{mn}^l) from the scattering coefficients (a_{mn}^l, b_{mn}^l), which need $\psi_n(x^l)$, $\psi_n(y^l)$, $D_n(x^l)$, and $D_n(y^l)$. $D_n(z)$ can simply be evaluated by the equation

$$D_n(z)=\frac{1}{p_n(z)}-\frac{n}{z}, \tag{36}$$

where $p_n(z)$ is the ratio function defined by $p_n(z)=\psi_n(z)/\psi_{n-1}(z)$, which can be computed recursively by its simple recurrence relation

$$p_n(z)=\frac{z}{2n+1-zp_{n+1}(z)}. \tag{37}$$

Starting from a sufficiently high order N for n with the asymptotic starting value

$$p_{N+1}(z)\sim\frac{z}{2n+3}, \tag{38}$$

the downward recurrence using Eq. (37) generates an accurate array of $p_n(z)$ from p_N to p_1. For the determination of the highest order N to assure a satisfactory numerical accuracy for the array $p_n(z)$, Wang and van de Hulst's suggestion is

$$N=1.1|z|+10,\ |z|\leqslant 10\,000, \tag{39a}$$

$$N=1.01|z|+10,\ |z|>10\,000. \tag{39b}$$

Our extensive test calculations show that Eqs. (39) are quite sufficient. Using any larger number of N than that given by Eqs. (39) does not change the numerical results of the array of $p_n(z)$ from a point of view of practical application. With the ratio functions calculated with sufficient precision, logarithm derivatives $D_n(z)$ can be computed by Eq. (36) and the Riccati-Bessel functions can be computed through the equation

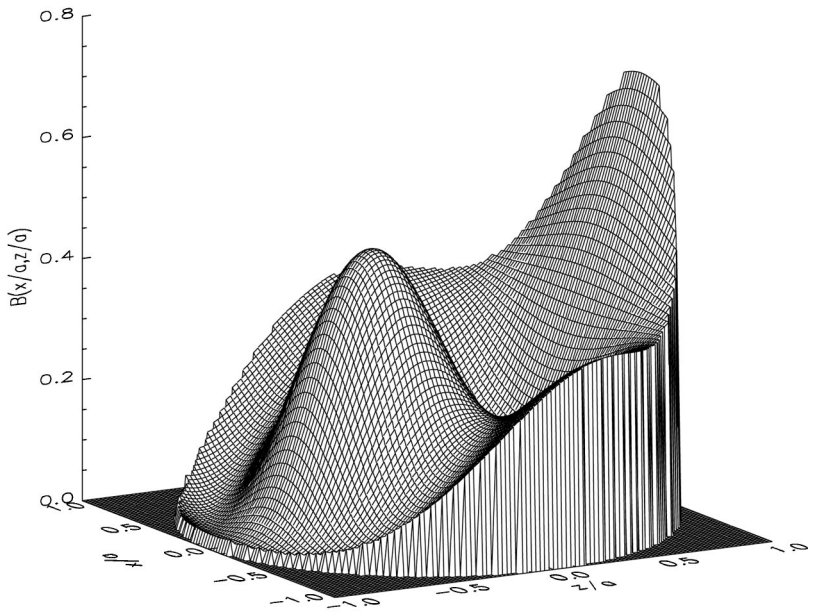

FIG. 1. Normalized source function for a sphere of radius a having the size parameter of 2.0 and the refractive index of $1.95-i0.66$. The distribution shown is for the cross section perpendicular to the electric vector of the monochromatic plane incident wave, the same as in all other figures throughout the present paper. This is the same sphere shown in Fig. 13 by Dusel *et al.* [14] and in Fig. 2 by Greene *et al.* [15].

$$\psi_n(z)=\psi_1(z)\prod_{j=2}^{n} p_j(z), \quad n\geqslant 2. \tag{40}$$

Here, $\psi_1(z)$ needs to be calculated directly. In general,

$$\psi_1(z)=\sum_{j=1}^{\infty}\frac{(-1)^{j+1}z^{2j}}{(2j+1)(2j-1)!}. \tag{41}$$

But as mentioned above, direct use of this expansion to calculate $\psi_1(z)$ is inadequate when $|z|$ is not small, no matter whether z is real or complex. For a real argument of $z=x$, when x is not small, $\psi_1(x)$ can be computed using the formula

$$\psi_1(x)=\frac{\sin x}{x}-\cos x, \tag{42}$$

and only when x is small (say, $|x|<0.1$), the expansion Eq. (41) can be used

$$\psi_1(x)\sim\sum_{j=1}^{4}(-1)^{j+1}x^{2j}\frac{2j}{(2j+1)!}, \tag{43}$$

which permits accurate calculation down to $x\sim 10^{-5}$ for the scattering calculation for spheres [39]. For a complex argument of $z=u+iv$, when $|z|$ is small (say, $|z|<0.1$), the evaluation of $\psi_1(z)$ can still use Eq. (43) by just replacing x by z in the equation. When $|z|$ is not small, $\psi_1(z)$ can be calculated by the equation

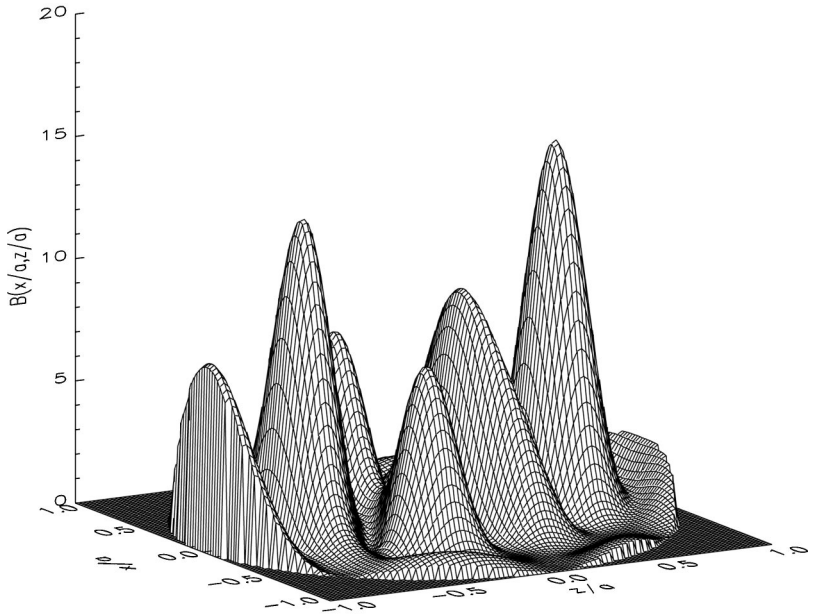

FIG. 2. Normalized source function for a sphere having the size parameter of 3.0 and the refractive index of $3.0-i0.01$. This is the same sphere shown in Fig. 8 by Dusel *et al.* [14].

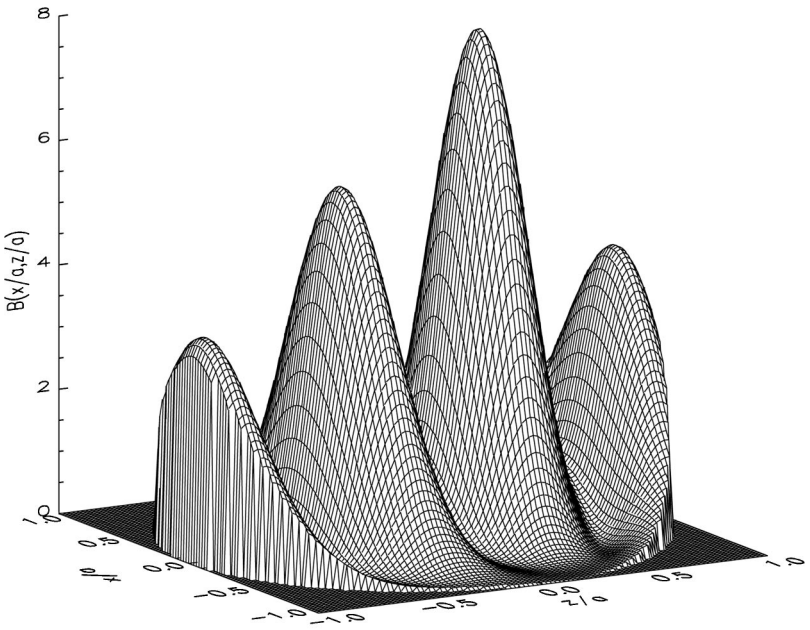

FIG. 3. Normalized source function for a sphere having the size parameter of 2.0 and the refractive index of $3.0-i0.01$. This is the same sphere shown in Fig. 10 by Dusel *et al.* [14].

$$\psi_1(z)=\frac{u\sin u\cosh v+v\cos u\sinh v}{u^2+v^2}-\cos u\cosh v$$
$$-i\left(\frac{v\sin u\cosh v-u\cos u\sinh v}{u^2+v^2}-\sin u\sinh v\right). \tag{44}$$

For a real argument x, $u=x$ and $v=0$, Eq. (44) reduces exactly to Eq. (42) because $\sinh v=0$ and $\cosh v=1$.

C. Evaluation of Mie scattering coefficients

Besides the vector translation coefficients $A_{mn\mu\nu}^{lj}$ and $B_{mn\mu\nu}^{lj}$, Eqs. (10) involve the Mie scattering coefficients a_n^j and b_n^j. The calculation of these Mie scattering coefficients using the ratio method has been discussed in detail by Wang and van de Hulst [39]. Using the ratio method, Wang and van de Hulst are able to compute efficiently and accurately the Mie scattering for a size parameter up to 50 000, which corresponds in visual light to a spherical particle of a diameter up to 6 mm. Similar to what given by Wang and van de Hulst [39], Eqs. (11) for the Mie scattering coefficients can be rewritten as

$$a_n^j=\left\{1-\frac{i\chi_n(x^j)[D_n(y^j)-m^jC_n(x^j)]}{\psi_n(x^j)[D_n(y^j)-m^jC_n(x^j)]}\right\}^{-1}, \tag{45a}$$

$$b_n^j=\left\{1-\frac{i\chi_n(x^j)[m^jD_n(y^j)-C_n(x^j)]}{\psi_n(x^j)[m^jD_n(y^j)-C_n(x^j)]}\right\}^{-1}, \tag{45b}$$

where, analogous to $D_n(x)$, $C_n(x)=\chi_n'(x)/\chi_n(x)$ is also a logarithmic derivative. Equations (45) are slightly different from those given by Wang and van de Hulst [39]. This is due

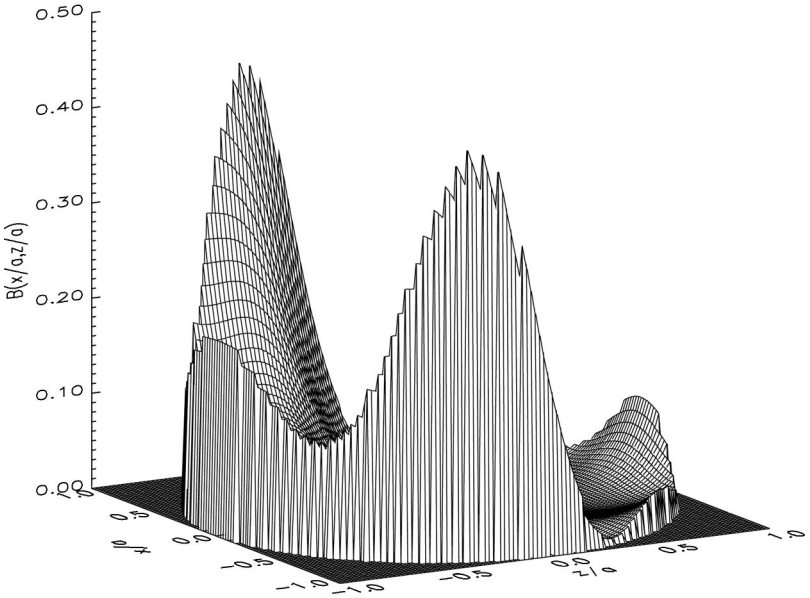

FIG. 4. Normalized source function for a sphere having the size parameter of 5.0 and the refractive index of $1.95-i0.66$. This is the same sphere shown in Fig. 16 by Dusel *et al.* [14].

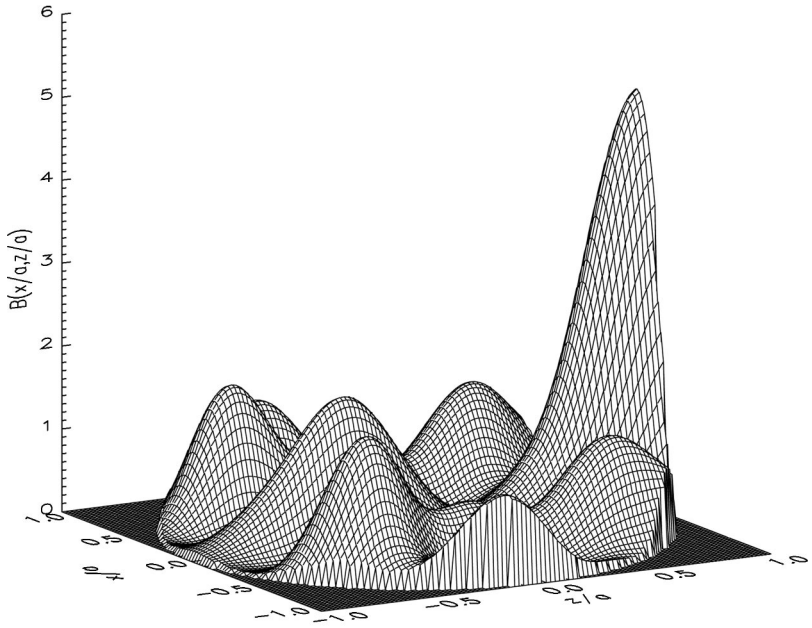

FIG. 5. Normalized source function for a sphere having the size parameter of 5.0 and the refractive index of $1.5-i0.1$. This is the same sphere shown in Fig. 3 by Greene *et al.* [15].

to our employment of the time factor $\exp(-i\omega t)$ instead of the $\exp(i\omega t)$ convention followed by Wang and van de Hulst.

Using Eqs. (45) to calculate a_n^j and b_n^j requires the values of $D_n(y^j)$, $C_n(x^j)$, $\psi_n(x^j)$, and $\chi_n(x^j)$. The method for the evaluation of $C_n(x)$ and $\chi_n(x)$ is slightly different from that for $D_n(x)$ and $\psi_n(x)$, which has also been discussed by Wang and van de Hulst [39]. Although $\chi_n(x)$ has the same form of recurrence relation as $\psi_n(x)$, it needs to emphasize that, unlike the computation of $p_n(x)$, which requires downward recurrence, the computation of the ratio function $q_n(x)$ array for $\chi_n(x)$ must use upward recurrence:

$$q_n(x)=\frac{\chi_n(x)}{\chi_{n-1}(x)}=\frac{2n-1}{x}-\frac{1}{q_{n-1}(x)}, \tag{46}$$

starting from $q_1(x)=1/x+\tan x$. Given the $q_n(x)$ array thus generated, $\chi_n(x)$ can be obtained from the equation

$$\chi_n(x)=\chi_1(x)\prod_{j=2}^{n} q_j(x), \quad n\geqslant 2, \tag{47}$$

with χ_1 computed using $\chi_1(x)=\cos x/x+\sin x$. Similar to the relation between $D_n(x)$ and the ratio function $p_n(x)$, the equation relating $C_n(x)$ with the ratio function $q_n(x)$ is

$$C_n(x)=\frac{\chi_n'(x)}{\chi_n(x)}=-\frac{n}{x}+\frac{1}{q_n(x)}. \tag{48}$$

D. Calculation of internal field components

In terms of the logarithmic derivative D_n, the equations for the internal electric field components of any lth sphere, Eqs. (21), can be rewritten as

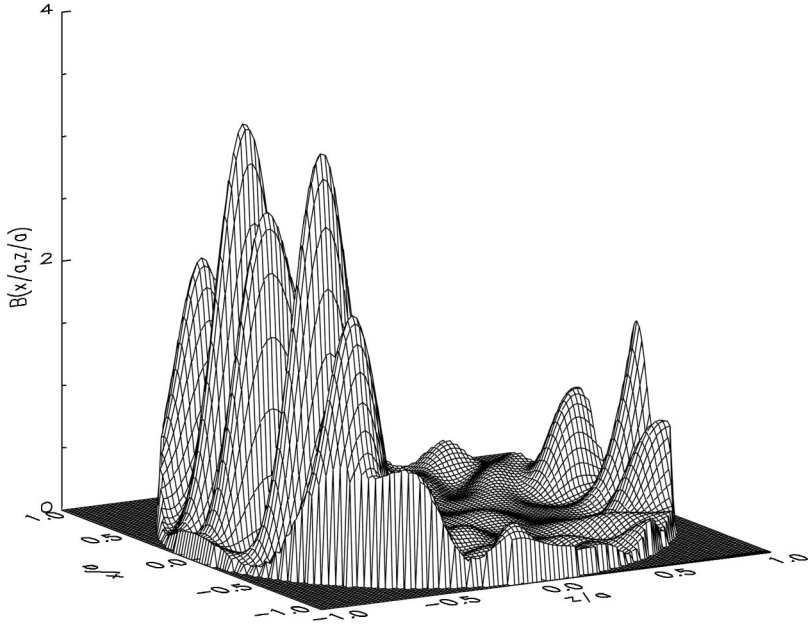

FIG. 6. Normalized source function for a sphere having the size parameter of 10.0 and the refractive index of $1.3-i0.1$. This is the same sphere shown in Fig. 4(c) by Greene *et al.* [15].

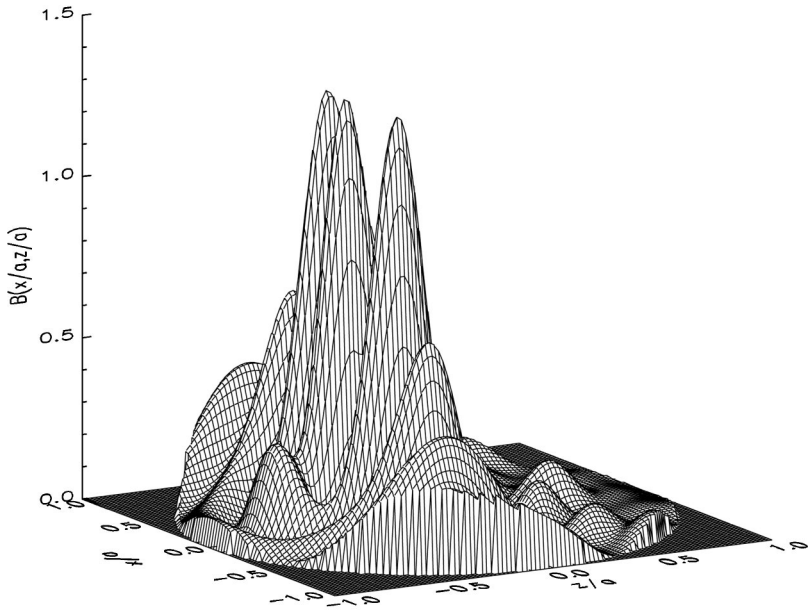

FIG. 7. Normalized source function for a sphere having the size parameter of 5.0 and the refractive index of $2.75-i0.2$. This is the same sphere shown in Fig. 5(b) by Greene *et al.* [15].

$$E_\theta^l = \sum_{n=1}^{N^l} \sum_{m=-n}^{n} E_{mn}(-id_{mn}^l D_n \tau_{mn} + c_{mn}^l \pi_{mn})\eta_n \rho^l \exp(im\phi^l), \tag{49a}$$

$$E_\phi^l = \sum_{n=1}^{N^l} \sum_{m=-n}^{n} E_{mn}(ic_{mn}^l \tau_{mn} + d_{mn}^l D_n \pi_{mn})\eta_n \rho^l \exp(im\phi^l), \tag{49b}$$

$$E_r^l = \sum_{n=1}^{N^l} \sum_{m=-n}^{n} -iE_{mn} n(n+1) d_{mn}^l P_n^m \eta_n \exp(im\phi^l), \tag{49c}$$

where the argument of D_n and η_n are $\rho^l = k^l r^l$ and the function η_n is defined by

$$\eta_n(\rho^l) = \frac{\psi_n(\rho^l)}{(\rho^l)^2} = \frac{j_n(\rho^l)}{\rho^l}. \tag{50}$$

To calculate these internal field components, one needs to compute the internal coefficients (d_{mn}^l, c_{mn}^l), the logarithmic derivative $D_n(\rho^l)$, and $\eta_n(\rho^l)$ at the specified ρ^l, as well as the angular functions π_{mn}, τ_{mn} and the Legendre function P_n^m. Recurrence relations of π_{mn} and τ_{mn} that can be used for their evaluation have been summarized by Xu [22]. Numerical aspects in the calculation of (d_{mn}^l, c_{mn}^l), $D_n(\rho^l)$ and $\eta_n(\rho^l)$ have been discussed in preceding sections. However, the origin of $\rho^l = 0$ is a special point, where any equation, in which ρ^l appears in the denominator, such as Eqs. (36), (42), (49), and (50), is not directly applicable. Nevertheless, Eqs. (49) have an alternative form

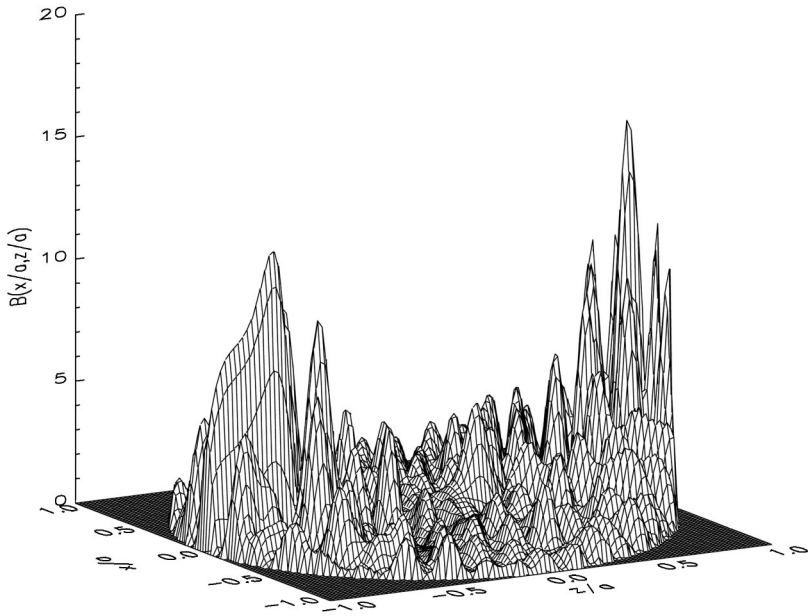

FIG. 8. Normalized source function for a sphere having the size parameter of 20.0 and the refractive index of $1.3-i0.01$. This is the same sphere shown in Fig. 6(a) by Greene *et al.* [15].

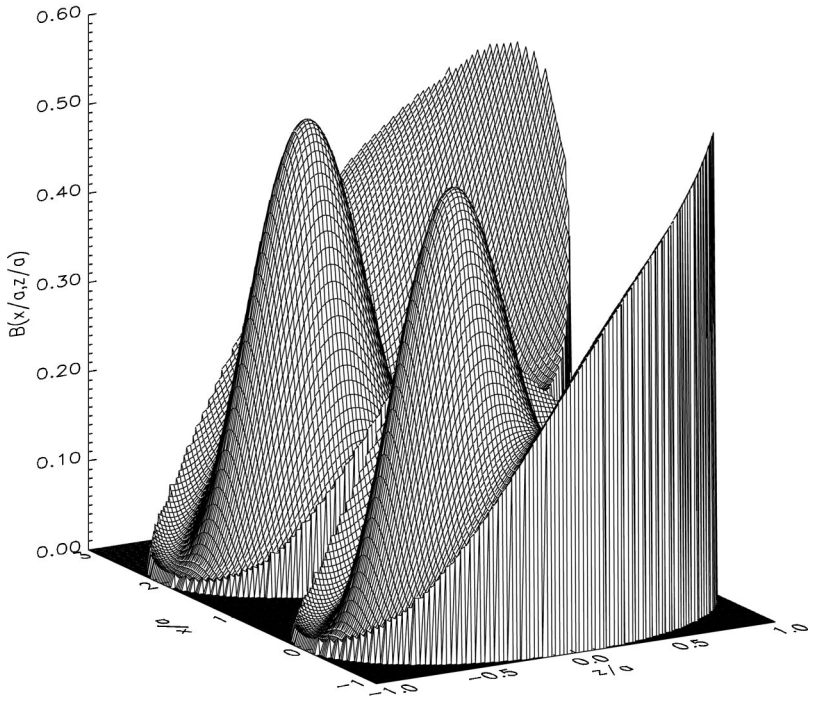

FIG. 9. Normalized source functions of two identical spheres in contact for the cross section in the *x*-*z* plane when the *z*-propagating incident plane wave is linearly *y* polarized. The spheres are in the orientation of *h*; their axis of symmetry lies in the scattering plane (the *x*-*z* plane) and perpendicular to the direction of propagation of the incident wave. The individual sphere is the same as that shown in Fig. 1.

$$E_\theta^l=\sum_{n=1}^{N^l}\sum_{m=-n}^{n}E_{mn}[-id_{mn}^l(\eta_n+j_n')\tau_{mn}+c_{mn}^l j_n\pi_{mn}]\exp(im\phi^l), \tag{51a}$$

$$E_\phi^l=\sum_{n=1}^{N^l}\sum_{m=-n}^{n}E_{mn}[ic_{mn}^l j_n\tau_{mn}+d_{mn}^l(\eta_n+j_n')\pi_{mn}]\exp(im\phi^l), \tag{51b}$$

$$E_r^l=\sum_{n=1}^{N^l}\sum_{m=-n}^{n}-iE_{mn}n(n+1)d_{mn}^l P_n^m\eta_n\exp(im\phi^l). \tag{51c}$$

It is easy to show that

$$j_1(0)=j_2(0)=\cdots=0, \tag{52a}$$

$$j_1'(0)=\frac{1}{3},\quad j_2'(0)=j_3'(0)=\cdots=0, \tag{52b}$$

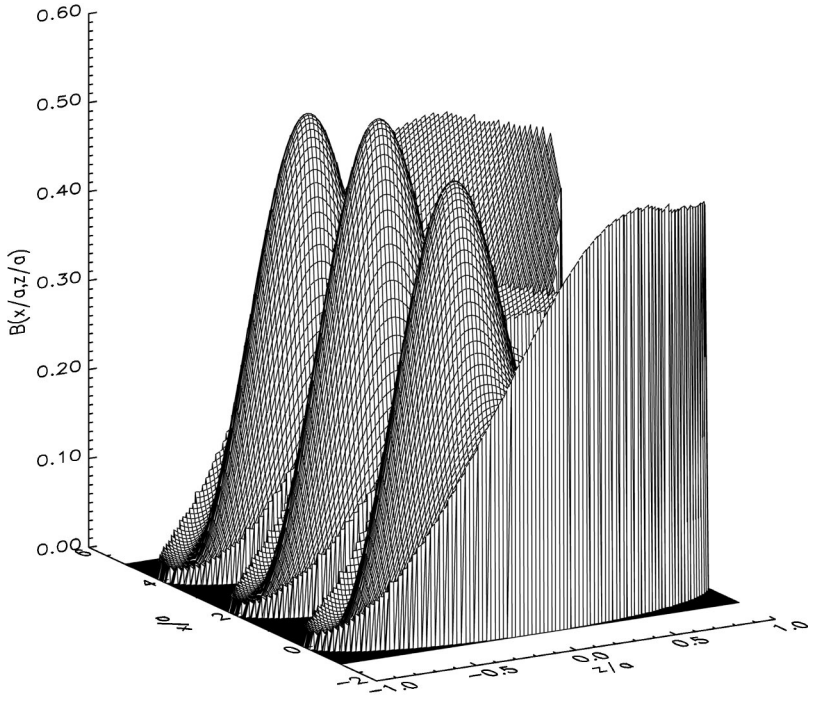

FIG. 10. Same as Fig. 9, but for a linear chain of three identical spheres.

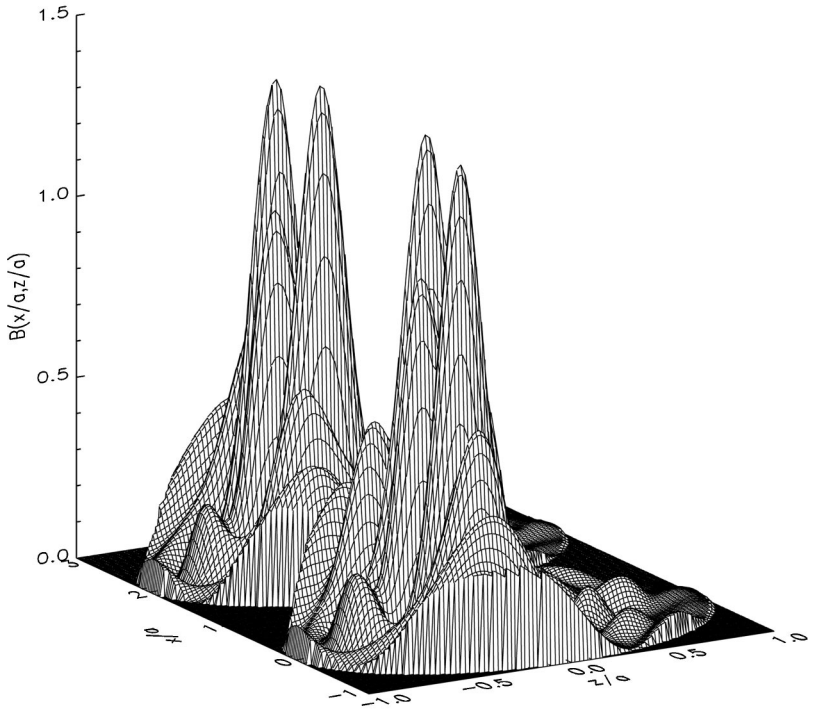

FIG. 11. Normalized source functions of two identical spheres in contact for the cross section in the *x*-*z* plane when the *z*-propagating incident plane wave is linearly *y* polarized. The spheres are in the orientation of *h*; their axis of symmetry lies in the scattering plane (the *x*-*z* plane) and perpendicular to the direction of propagation of the incident wave. The individual sphere is the same as that shown in Fig. 7.

$$\eta_1(0)=\frac{1}{3},\quad \eta_2(0)=\eta_3(0)=\cdots=0. \tag{52c}$$

Using Eqs. (51) and (52), as well as the special values,

$$E_{-11}=6iE_0,\quad E_{01}=3iE_0,\quad E_{11}=\frac{3}{2}iE_0, \tag{53a}$$

$$\tau_{-11}=-\frac{\cos\theta}{2},\quad \tau_{01}=-\sin\theta,\quad \tau_{11}=\cos\theta, \tag{53b}$$

$$\pi_{-11}=\frac{1}{2},\quad \pi_{01}=0,\quad \pi_{11}=1, \tag{53c}$$

$$P_1^{-1}=-\frac{\sin\theta}{2},\quad P_1^0=\cos\theta,\quad P_1^1=\sin\theta, \tag{53d}$$

we obtain the analytical expressions for the field components at the origin:

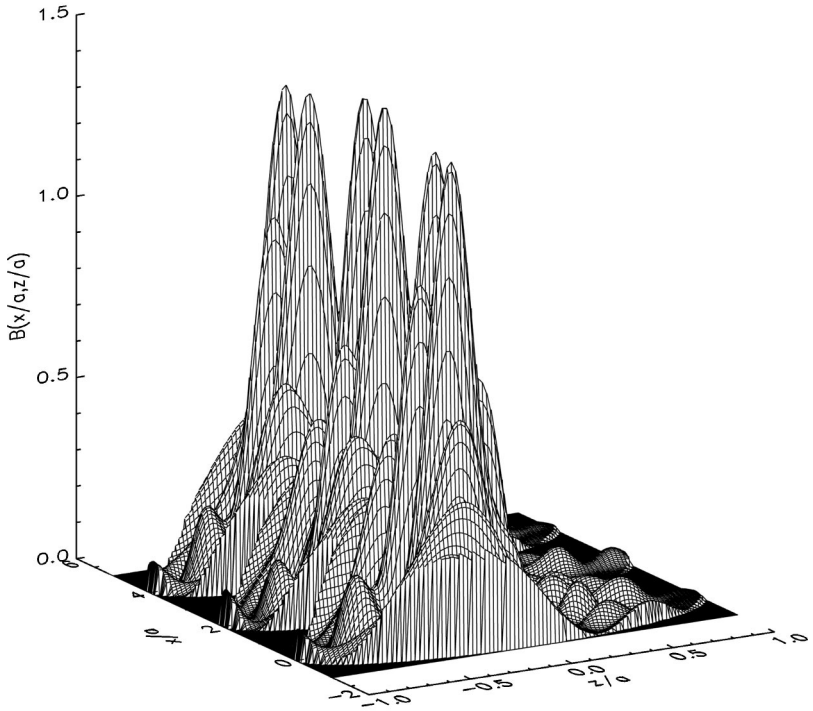

FIG. 12. Same as Fig. 11, but for a linear chain of three identical spheres.

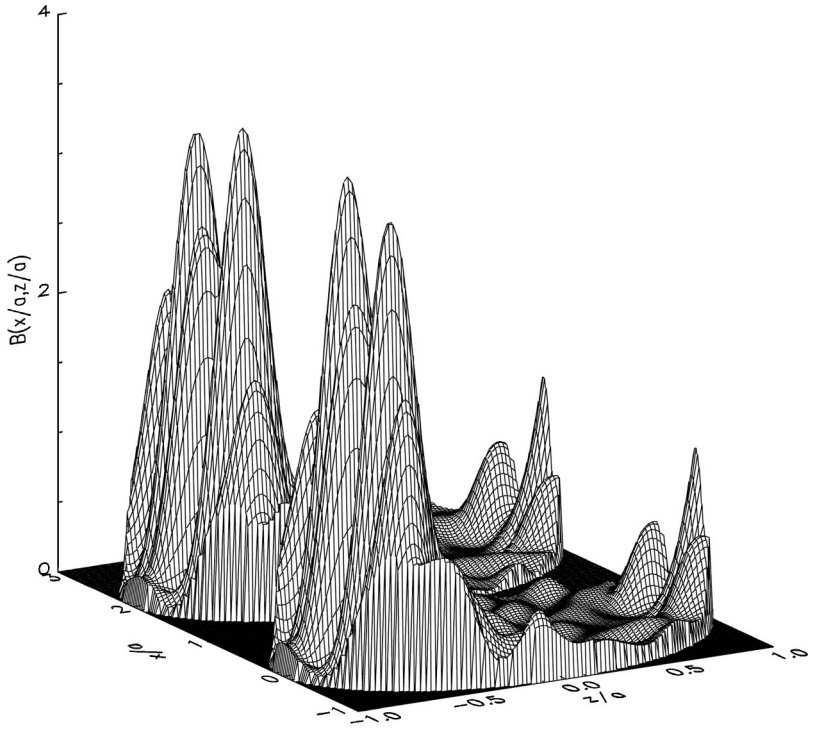

FIG. 13. Normalized source functions of two identical spheres in contact for the cross section in the *x*-*z* plane when the *z*-propagating incident plane wave is linearly *y* polarized. The spheres are in the orientation of *h*; their axis of symmetry lies in the scattering plane (the *x*-*z* plane) and perpendicular to the direction of propagation of the incident wave. The individual sphere is the same as that shown in Fig. 6.

$$E_{\theta}^{l}|_{r=0}=E_0\frac{d_1^l}{a_1^l}[(-2a_{-11}^l+a_{11}^l)\cos\theta\cos\phi-2a_{01}^l\sin\theta+i(2a_{-11}^l+a_{11}^l)\cos\theta\sin\phi], \tag{54a}$$

$$E_{\phi}^{l}|_{r=0}=E_0\frac{d_1^l}{a_1^l}[i(2a_{-11}^l+a_{11}^l)\cos\phi+(2a_{-11}^l-a_{11}^l)\sin\phi], \tag{54b}$$

$$E_{r}^{l}|_{r=0}=E_0\frac{d_1^l}{a_1^l}[(-2a_{-11}^l+a_{11}^l)\sin\theta\cos\phi+2a_{01}^l\cos\theta+i(2a_{-11}^l+a_{11}^l)\sin\theta\sin\phi]. \tag{54c}$$

When $L=1$, i.e., for a single sphere,

$$a_{-11}=-\frac{a_1}{4}\exp(i\beta),\quad a_{01}=0,\quad a_{11}=\frac{a_1}{2}\exp(-i\beta), \tag{55}$$

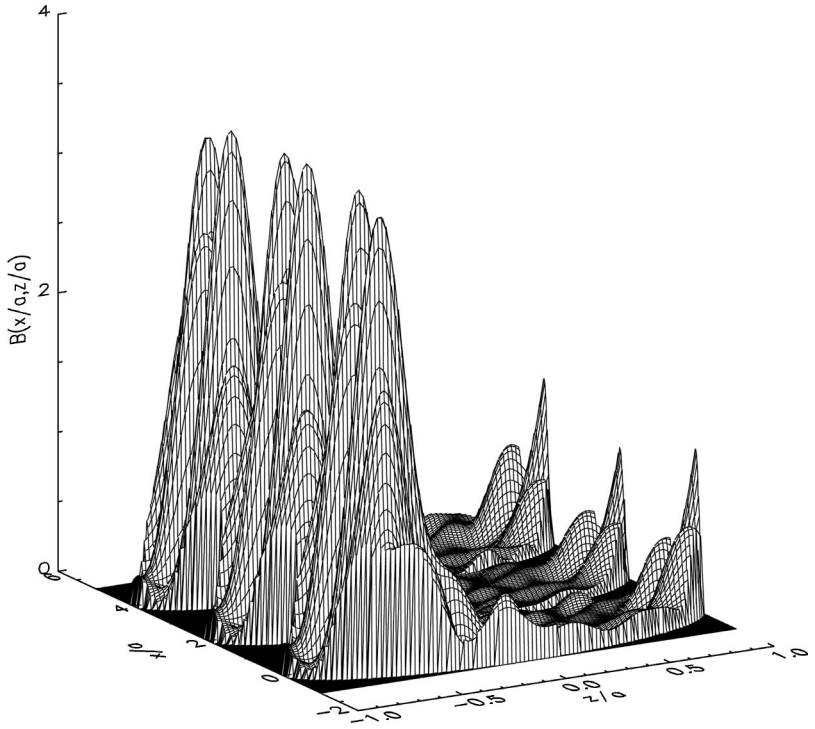

FIG. 14. Same as Fig. 13, but for a linear chain of three identical spheres.

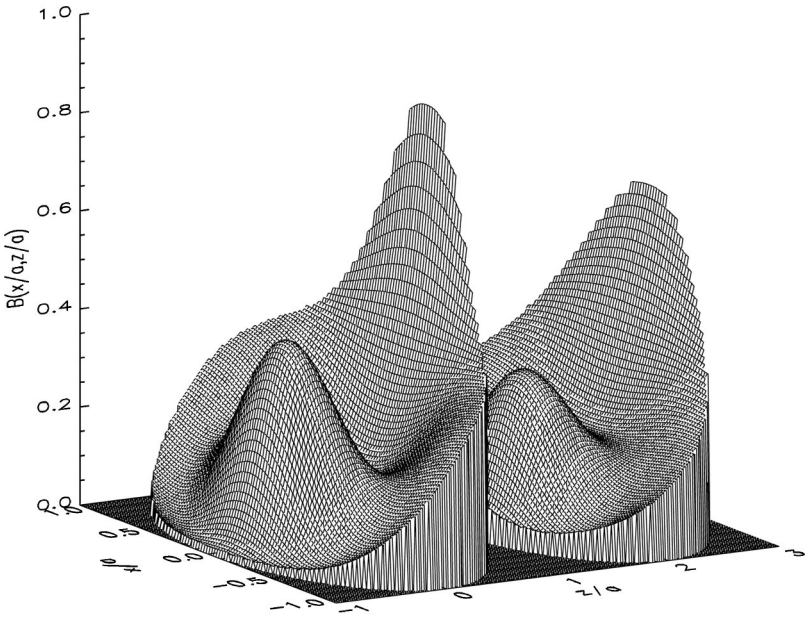

FIG. 15. Normalized source functions of two identical spheres in contact for the cross section in the *x*-*z* plane when the *z*-propagating incident plane wave is linearly *y* polarized. The spheres are in the orientation of *k*; their axis of symmetry is parallel to the *z* axis, i.e., the direction of propagation of the incident wave. The individual sphere is the same as that shown in Fig. 1.

and Eqs. (54) reduce to

$$\begin{pmatrix} E_r|_{r=0} \\ E_\theta|_{r=0} \\ E_\phi|_{r=0} \end{pmatrix} = E_0 d_1 \begin{pmatrix} \cos(\phi-\beta)\sin\theta \\ \cos(\phi-\beta)\cos\theta \\ -\sin(\phi-\beta) \end{pmatrix}. \qquad (56)$$

Equation (56) shows that, for a single Mie sphere, the electric vector at the sphere center is parallel to the incident electric vector and has a magnitude of $E_0 d_1$.

IV. NUMERICAL RESULTS

Armed with the formulas and numerical techniques discussed in the preceding sections, it is feasible to accurately calculate the heat-source function of aggregated spheres, including, of course, isolated single Mie spheres. In this section, we first compare our numerical results for the normalized source function of single spheres with those published by Dusel *et al.* [14] and Greene *et al.* [15] and then present our results for aggregates of spheres.

A. Single spheres

Dusel *et al.* [14] in 1979 and Greene *et al.* [15] in 1985 reported the results of their study on the distribution of absorption centers within single Mie spheres. To provide a qualitative impression on the source function of Mie spheres, both the authors presented topographical perspective views of the distribution of the normalized source function in the equatorial plane ($x=0$, i.e., in the *y*-*z* plane) when the *z*-propagating incident plane wave is *x* polarized (i.e., $\beta=0°$). For the Mie case, this equatorial-plane distribution is the same as in the *x*-*z* plane when the incident plane wave is *y* polarized (i.e., $\beta=90°$). Generally, it is the same distribution as in the plane perpendicular to the incident electrical vector when the incident wave has an arbitrary linear polarization angle β. We have compared our numerical solutions with all those published by Dusel *et al.* and Greene *et al.* Our results are in reasonable agreement with those by Dusel *et al.* despite discrepancies in some cases. But there are in general significant discrepancies between Greene *et al.*'s and our results, which usually show little resemblance. The probable reason for the discrepancies has been mentioned in Sec.

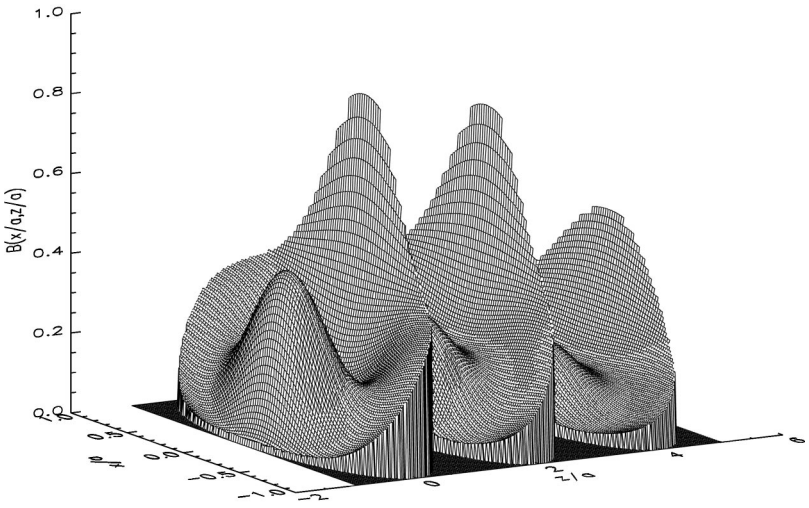

FIG. 16. Same as Fig. 15, but for a linear chain of three identical spheres.

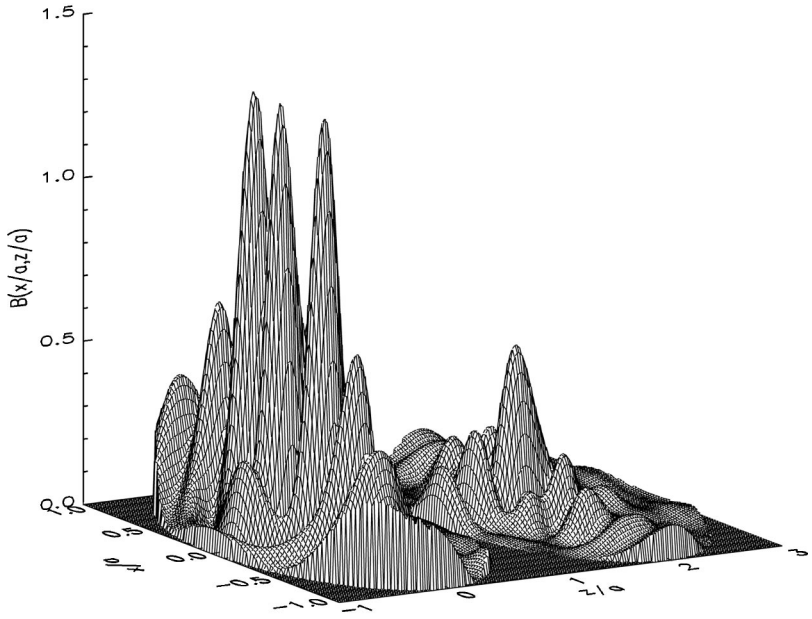

FIG. 17. Normalized source functions of two identical spheres in contact for the cross section in the *x*-*z* plane when the *z*-propagating incident plane wave is linearly *y* polarized. The spheres are in the orientation of *k*; their axis of symmetry is parallel to the *z* axis, i.e., the direction of propagation of the incident wave. The individual sphere is the same as that shown in Fig. 7.

III B, which are perhaps due to the use of different numerical techniques in the calculation of Riccati-Bessel functions. Numerical errors in the evaluation of the functions may distort completely the source function. As an example, we present in Fig. 1 our result for a Mie sphere having the size parameter of 2.0 and the refractive index of $1.95-i0.66$. It should be pointed out here that the negative sign for the imaginary part of the refractive index is normally used in the case of time dependence of electromagnetic field being $\exp(i\omega t)$. But we use the convention of $\exp(-i\omega t)$ instead. Strictly speaking, in our case we should have a positive imaginary part for the refractive index. We use negative sign throughout this paper in keeping with Dusel *et al.* and Greene *et al.* because we compare these authors' results with ours. With this in mind, it will cause no confusion. Figure 1 shows the distribution of the normalized heat-source function in the *x*-*z* plane when the *z*-propagating incident plane wave is *y* polarized, the same as in all other figures throughout this paper. Exactly the same sphere has been calculated by both Dusel *et al.* [14] and Greene *et al.* [15]. Compared with Fig. 13 in the article by Dusel *et al.* and with Fig. 2 in the article by Greene *et al.*, it is clear that our result is quite different. While Dusel *et al.*'s source function for the sphere shows three distinct peaks, Greene *et al.*'s and ours for the same sphere have only two peaks. Interestingly, if there were no peak at the illuminated side and only two peaks remained in Dusel *et al.*'s result, Dusel *et al.*'s and our source functions for this sphere would look alike. As noticed by Greene *et al.*, Dusel *et al.*'s source function containing three areas of absorption yields a symmetrical temperature distribution and thus a small photophoretic force. Both Greene *et al.*'s and our source functions indicate larger photophoretic forces due to an uneven temperature distribution. It is noted that, however, the photophoretic forces predicted based on the source functions calculated respectively by Greene *et al.* and by us have opposite directions. This is because, although both have two areas of absorption, the locations of the two absorption peaks are totally different. Greene *et al.* find the higher peak at the illuminated side and that of ours is at the shaded side. A positive photophoresis for this case is predicted by Greene *et al.*'s result. But it is negative, predicted by our result. In some range of the combination of particle size and refractive index, a not highly absorptive particle, acting like a microlens, may focus input radiation to the rear side of the particle,

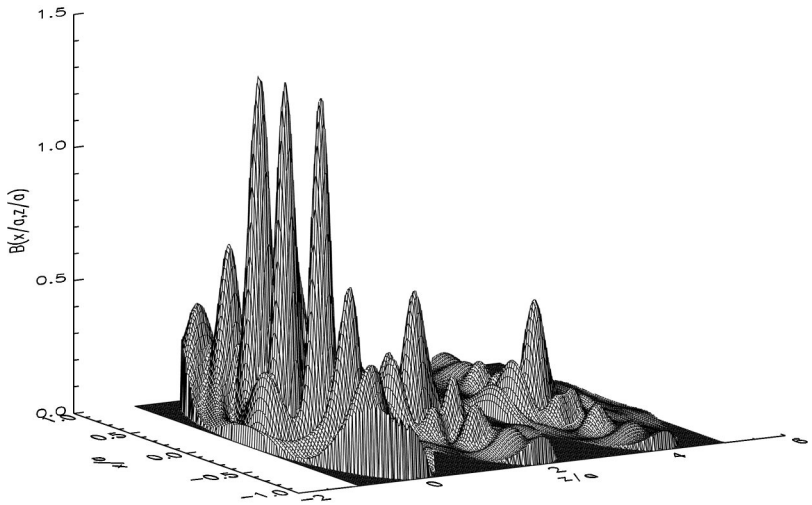

FIG. 18. Same as Fig. 17, but for a linear chain of three identical spheres.

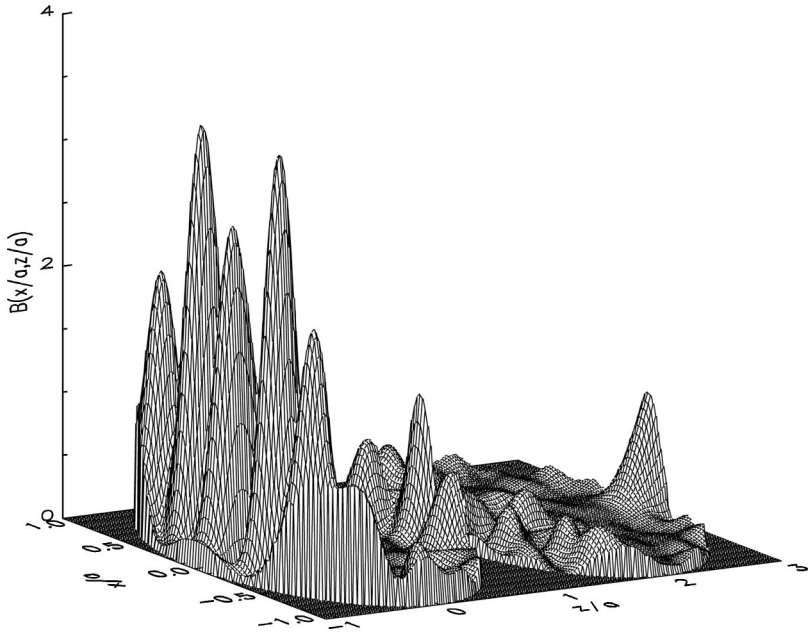

FIG. 19. Normalized source functions of two identical spheres in contact for the cross section in the *x*-*z* plane when the *z*-propagating incident plane wave is linearly *y* polarized. The spheres are in the orientation of *k*; their axis of symmetry is parallel to the *z* axis, i.e., the direction of propagation of the incident wave. The individual sphere is the same as that shown in Fig. 6.

leaving a hotter back surface and resulting in a negative photophoresis. But a small change in the particle size and/or refractive index may cause a reversal of the direction. Generally, the internal field distribution and thus the direction of the photophoretic force are highly dependent on the physical parameters of the particles, changing from particle to particle.

Figures 2 and 3 are two examples showing that the source functions calculated by Dusel *et al.* for the single spheres are fairly close to ours. These figures correspond, respectively, to Figs. 8 and 10 of Dusel *et al.* [14] and show an overall fairly good agreement in predicting the characteristics of the source functions, i.e., the number, the locations, and the relative strengths of the absorption peaks. We note that the size parameters of these spheres do not exceed 3.0. When the size parameter of a sphere becomes larger, there appear obvious differences between Dusel *et al.*'s and our results. Such an example is shown in Fig. 4 that refers to a sphere of refractive index $1.95-i0.66$ having the size parameter of 5.0. While the profile of the source function shown in Fig. 4 has in some respects a resemblance to the result in Fig. 16 of Dusel *et al.*, two peaks showing up at both the illuminated and the shaded sides, there are also clear differences. Our calculation brings out the prominent peaks at both wing sides. For a larger size parameter, the calculation of the source function requires the evaluation of higher orders and degrees Riccati-Bessel functions, which may cause larger numerical errors. This may be the reason that some approximations work reasonably well at low order function calculations and are not sufficiently accurate at higher orders.

Figures 5–8 are our results for the normalized source functions of four more Mie spheres. These spheres have also been calculated by Greene *et al.* [15] and correspond respectively to Figs. 3, 4c, 5b, and 6a in their article. Significant discrepancies can be found between Greene *et al.*'s and our results. This may be, in our opinion, mainly because the size parameters of the spheres calculated by Greene *et al.* are all large, ranging from 3 to 20. Numerical errors easily destroy the accuracy of numerical solutions for large spheres. In other examples calculated by Greene *et al.*, there are some spheres having a large value of the imaginary part of the refractive index. For these highly absorptive particles, the

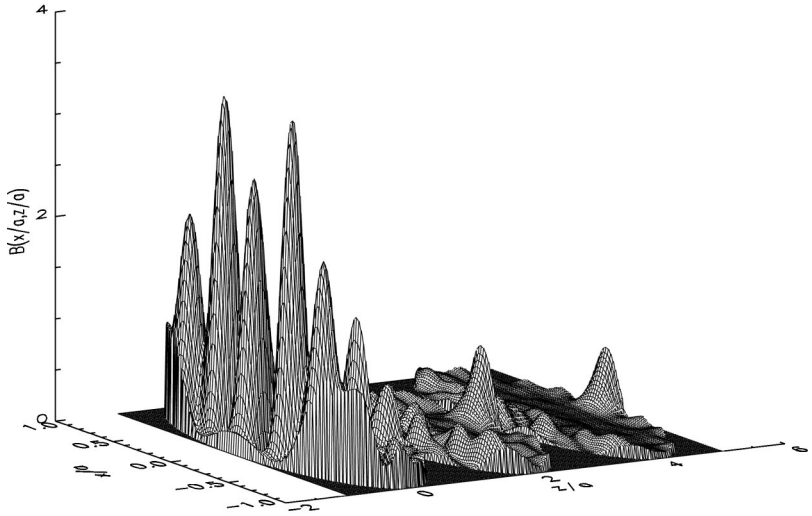

FIG. 20. Same as Fig. 19, but for a linear chain of three identical spheres.

incident radiation can hardly penetrate and absorption occurs all along the particle surface. Usually, for highly absorptive particles of a large size there occurs only front surface absorption, leading to a positive photophoresis.

B. Aggregated spheres

For a sphere in an aggregate, interaction with other spheres in the aggregate alters its internal field. The ''actual'' incident waves for a sphere in an aggregate include the scattered waves from all other spheres in the aggregate and its internal field changes accordingly from that when it is isolated, i.e., the Mie field. The extent to which the internal field of a sphere deviates from its internal Mie field is determined by its degree of interaction with other spheres, which is the synthetic effect of orientation, size, composition, and configuration of the spheres. Figures 9–14 refer to six aggregates of spheres: three dumbbells and three linear three-sphere chains. All component spheres in each of the aggregates are identical and all adjacent spheres are in contact. In Figs. 9–14, the orientation of the aggregates of spheres is such that their axis of symmetry is parallel to the x axis, i.e., perpendicular to the direction of propagation of the initial incident plane wave and in the scattering plane. This orientation is referred to as the orientation h. In Figs. 9 and 10, the individual sphere is the same as that shown in Fig. 1, i.e., the size parameter of 2 and the refractive index of $1.95 - i0.66$. The individual sphere in the aggregates shown in Figs. 11 and 12 corresponds to that in Fig. 7 and for Figs. 13 and 14 it is the same as that in Fig. 6. Compared respectively with Figs. 1, 7, and 6, Figs. 9–14 show that, when spheres are aligned along the x axis, the internal fields remain similar to those when the spheres are isolated, although it is perturbed to varying degrees, depending on the size and the refractive index of the spheres. For the aggregates of two identical spheres in contact in the orientation of h, the two internal fields are symmetric about the point of contact of the spheres. For the aggregates of three identical spheres, the internal field of the middle sphere changes the most. Figures 15–20 are respectively the same as Figs. 9–14 except that the aggregates of spheres are in the orientation of k, which means that the spheres are now aligned along the z axis, i.e., the axis of symmetry of the spheres is parallel to the incident direction. In this orientation k, the strongest interaction between spheres takes place. Compared again respectively with Figs. 1, 7, and 6, Figs. 15–20 clearly show that the internal fields of the spheres not directly exposed to the incident radiation deviate significantly from those when the spheres are isolated. This results from the strong interaction between spheres. The results shown here tell us that the internal fields of the spheres in an aggregate are strongly configuration and orientation dependent.

V. REMARKS

In many practical scientific problems concerning radiative scattering by small particles, of interest are the scattering quantities derivable from the scattered radiation from the particles. However, there are cases where the detailed knowledge about the electromagnetic fields inside the scattering particles is desirable. Photophoresis of the gas-suspended small particles is one of such examples for the practical application of the internal field. The distribution of heat-source function within an illuminated particle, the basis for photophoresis, is completely determined by the internal field of the particle. As described here, the internal field distribution can now be precisely predicted for an arbitrary ensemble of homogeneous spheres, based on the rigorous analytic solution to the multisphere-scattering problem, which includes the Mie theory for a single sphere as the simplest special case. In addition to the rigorous and practically applicable formulation, to obtain a sufficiently accurate internal field distribution for spherical particles in practical calculations, reliable numerical techniques are of importance as well. Moderate numerical errors in the evaluation of the special functions involved may lead to a misleading numerical solution. As mentioned by Greene *et al.* [15], reduction of the normalized error in the Riccati-Bessel functions from 10^{-5} to 10^{-16} has a major effect on the source function generated. We have discussed here the necessary numerical schemes adequate for a practical use. There are fairly good approximations in predicting internal field distribution for small and large size particles or some other special cases. Highly accurate numerical solutions obtained by rigorous calculations can be used to test the accuracy and limitations of the approximations.

As shown in Figs. 1–8, the normalized source function, equivalently, the distribution of the internal field, of a Mie sphere depends strongly on the size parameter and the complex refractive index of the sphere. The pattern of the distribution of absorption centers in a sphere changes dramatically with the change in size and/or refractive index. This is just as different spheres have totally different profiles of the phase function, i.e., the angular distribution of the polarization components of scattered intensity. The scattering coefficients, i.e., the multipole expansion coefficients of the scattered field (a_{mn}, b_{mn}) vary with the size and the refractive index of a sphere. Equations (20) clearly show that the internal coefficients, i.e., the multipole expansion coefficients of the internal field (d_{mn}, c_{mn}) change with (a_{mn}, b_{mn}) in a more complex manner. For aggregated spheres, the interaction between spheres alters the scattering patterns of the individual spheres and makes the situation even more complicated. The internal field distribution of an individual sphere in an aggregate is usually quite different from its internal Mie field, unless the sphere is sufficiently distant from all other spheres in the aggregate so that it can be considered as isolated due to the very weak and thus negligible interaction with other spheres. In general, internal field distributions of aggregated spheres depend strongly on the configuration and orientation of their ensemble.

Scattering theories, especially those developing, such as the recent multisphere light-scattering theory [22–24], are subject to stringent experimental and numerical tests. Mie theory has been incontrovertibly proved by every piece of evidence in its practical applications. Experimental tests of the multisphere-scattering theory have been so far successful [25,26]. However, unlike the distribution of scattered field, which is directly measurable and a systematic experimental scrutiny can be performed, direct comparison between theoretical and experimental results for the internal field is difficult. Related physical phenomena, such as photophoresis, can only be used to test the correctness of the prediction from theoretical calculations in an indirect way and to a lim-

ited extent. In practice, the reliability of the numerical solution of the internal field depends largely on the accuracy of the numerical schemes used in its calculation. Greene *et al.* [15] have discussed the link between the numerical errors in evaluating Riccati-Bessel functions and the errors in calculating the absorption cross section and the asymmetry factor of the temperature distribution on particle surface through volumetric integration of the source function (see, especially, Fig. 7 in Ref. [15]). These authors suggested that, in calculating the source function, the Riccati-Bessel functions must be accurate to at least six (preferably eight or ten) significant figures. They concluded that, if the accuracy of these functions is insufficient, the resultant source function will be grossly incorrect. As mentioned by Dusel *et al.* [14], the accuracy of the calculated Riccati-Bessel functions can be inspected by corresponding criteria, for example, the following expression can be used for $\psi_n(z)$:

$$\sum_{n=1}^{\infty} (2n+1) j_n^2(z) = 1. \tag{57}$$

We have tested our calculations related to the results presented in this paper. For $\psi_n(z)$, the residuals, defined by

$$R = \left| 1 - \sum_{n=1}^{\infty} (2n+1) j_n^2(z) \right|, \tag{58}$$

are all sufficiently small ($R < 10^{-12}$). Similar tests can be used for other special functions involved. Dusel *et al.* [14] and Greene *et al.* [15] also tested their results by integrating the source function over the entire volume of the scattering particle and then comparing the result with the absorption cross section calculated using the Mie formula. For any individual sphere in an ensemble of spheres, a similar test applies. A rigorous analytical expression for the absorption cross section of any component sphere has been given in the literature, e.g., Ref. [23]. In principle, the absorption cross section obtained from the rigorous expression should be identical to that obtained by the integration of the source function over the volume of the particle. However, in practical calculations, the integration result is largely determined by dominant absorption areas and the accuracy of the numerical integration is also affected by the numerical method and the grid of data points used in the integration. In our test calculations, the absorption cross sections obtained from the rigorous expression and the integration are in reasonable agreement, depending on the step size used in the integration.

With the use of the numerical techniques described here, reliable Mie computations are feasible for the size parameter up to 50 000 at least [39]. In principle, the same applies to aggregated spheres. In multisphere calculations, however, the largest size parameter is limited by the computation of the vector translation coefficients $A_{mn\mu\nu}^{lj}$ and $B_{mn\mu\nu}^{lj}$. The numerical values of $A_{mn\mu\nu}^{lj}$ and $B_{mn\mu\nu}^{lj}$ increase rapidly with increasing n and/or ν. When n and ν reach ~ 45, which corresponds roughly to the size parameter 30 for an individual sphere, the numerical values of $A_{mn\mu\nu}^{lj}$ and $B_{mn\mu\nu}^{lj}$ overflow double-precision floating point representation. In multisphere calculations, higher-precision (higher than double) arithmetic must be used if a larger size parameter (>30 approximately) is desired.

ACKNOWLEDGMENT

This study was supported in part by the National Science Foundation through Grant No. AST-9619539.

[1] F. Ehrenhaft, Phys. Z. **18**, 352 (1917).
[2] A. Rubinowitz, Ann. Phys. (Leipzig) **62**, 691 (1920).
[3] G. Hettner, Z. Phys. **37**, 179 (1926).
[4] P. Epstein, Z. Phys. **54**, 537 (1929).
[5] R. Whytlaw-Gray and H. S. Patterson, *Smoke: A Study of Aerial Disperse Systems* (Edward Arnold, London, 1932).
[6] M. Reiss, Phys. Z. **33**, 185 (1932).
[7] F. Ehrenhaft, J. Franklin Inst. **233**, 235 (1942).
[8] F. Geguillon, C. R. Hebd. Seances Acad. Sci. **231**, 274 (1950).
[9] C. Orr, Jr. and E. Y. H. Keng, J. Atmos. Sci. **21**, 475 (1964).
[10] S. Arnold and Y. Amani, Opt. Lett. **5**, 242 (1980).
[11] J. A. Stratton, *Electromagnetic Theory* (McGraw-Hill, New York, 1941), p. 137.
[12] M. Kerker and D. D. Cooke, Appl. Opt. **12**, 1378 (1973).
[13] M. Kerker and D. D. Cooke, J. Opt. Soc. Am. **72**, 1267 (1982).
[14] P. W. Dusel, M. Kerker, and D. D. Cooke, J. Opt. Soc. Am. **69**, 55 (1979).
[15] W. M. Greene, R. E. Spjut, E. Bar-Ziv, A. F. Sarofim, and J. P. Longwell, J. Opt. Soc. Am. B **2**, 998 (1985).
[16] L. V. Lorenz, in *Oeuvres Scientifiques de L. Lorenz*, revues et annotées par H. Valentiner (Librairie Lehman et Stage, Copenhagen, 1898), p. 405.
[17] G. Mie, Ann. Phys. (Leipzig) **25**, 377 (1908).
[18] P. Debye, Ann. Phys. (Leipzig) **30**, 57 (1909).
[19] H. C. van de Hulst, *Light Scattering by Small Particles* (Wiley, New York, 1957).
[20] M. Kerker, *The Scattering of Light and Other Electromagnetic Radiation* (Academic, New York, 1969).
[21] C. F. Bohren and D. R. Huffman, *Absorption and Scattering of Light by Small Particles* (Wiley, New York, 1983).
[22] Y.-l. Xu, Appl. Opt. **34**, 4573 (1995); **37**, 6494 (1998).
[23] Y.-l. Xu, Appl. Opt. **36**, 9496 (1997).
[24] Y.-l. Xu, Phys. Lett. A **249**, 30 (1998).
[25] Y.-l. Xu and B. Å. S. Gustafson, Appl. Opt. **36**, 8026 (1997).
[26] Y.-l. Xu and R. T. Wang, Phys. Rev. E **58**, 3931 (1998).
[27] W. J. Wiscombe, Appl. Opt. **19**, 1505 (1980).
[28] A. Stein, Q. Appl. Math. **19**, 15 (1961).
[29] O. R. Cruzan, Q. Appl. Math. **20**, 33 (1962).
[30] Y.-l. Xu, J. Comput. Phys. **139**, 137 (1998).
[31] B. Friedman and J. Russek, Q. Appl. Math. **12**, 13 (1954).
[32] E. P. Wigner, in *Quantum Theory of Angular Momentum*, edited by L. C. Biedenharn and H. van Dam (Academic Press, New York, 1965), p. 89.
[33] J. A. Gaunt, Philos. Trans. R. Soc. London, Ser. A **228**, 151 (1929).

[34] Y.-l. Xu, J. Comput. Phys. **127**, 285 (1996); **134**, 200 (1997).
[35] Y.-l. Xu, Math. Comput. **65**, 1601 (1996).
[36] Y.-l. Xu, J. Comput. Appl. Math. **85**, 53 (1997).
[37] W. D. Ross, Appl. Opt. **11**, 1919 (1972).
[38] W. J. Lentz, Appl. Opt. **15**, 668 (1976).
[39] R. T. Wang and H. C. van de Hulst, Appl. Opt. **30**, 106 (1991).
[40] R. T. Wang and H. C. van de Hulst, Appl. Opt. **34**, 2811 (1995).